High throughput system for magnetic manipulation of cells, polymers, and biomaterials

Richard Chasen Spero,[1] Leandra Vicci,[2] Jeremy Cribb,[3] David Bober,[4] Vinay Swaminathan,[5] E. Timothy O'Brien,[1] Stephen L. Rogers,[6] and R. Superfine[1,a)]
[1]*Department of Physics and Astronomy, University of North Carolina at Chapel Hill, 141 Phillips Hall, CB #3255, Chapel Hill, North Carolina 27599, USA*
[2]*Department of Computer Science, University of North Carolina at Chapel Hill, Sitterson Hall, CB # 3175, Chapel Hill, North Carolina 27599, USA*
[3]*Department of Biomedical Engineering, University of North Carolina at Chapel Hill, 152 MacNider Hall, CB #7575, Chapel Hill, North Carolina 27599, USA*
[4]*Swarthmore College, 500 College Avenue, Swarthmore, Pennsylvania 19081, USA*
[5]*Curriculum in Applied and Materials Sciences, University of North Carolina at Chapel Hill, 141 Chapman Hall, CB #3287, Chapel Hill, North Carolina 27599, USA*
[6]*Department of Biology and the Carolina Genome Science Center, University of North Carolina at Chapel Hill, 421 Fordham Hall, CB #3280, Chapel Hill, North Carolina 27599, USA*

(Received 27 June 2008; accepted 4 August 2008; published online 29 August 2008)

In the past decade, high throughput screening (HTS) has changed the way biochemical assays are performed, but manipulation and mechanical measurement of micro- and nanoscale systems have not benefited from this trend. Techniques using microbeads (particles $\sim 0.1-10$ μm) show promise for enabling high throughput mechanical measurements of microscopic systems. We demonstrate instrumentation to magnetically drive microbeads in a biocompatible, multiwell magnetic force system. It is based on commercial HTS standards and is scalable to 96 wells. Cells can be cultured in this magnetic high throughput system (MHTS). The MHTS can apply independently controlled forces to 16 specimen wells. Force calibrations demonstrate forces in excess of 1 nN, predicted force saturation as a function of pole material, and powerlaw dependence of $F \sim r^{-2.7\pm0.1}$. We employ this system to measure the stiffness of SR2+ *Drosophila* cells. MHTS technology is a key step toward a high throughput screening system for micro- and nanoscale biophysical experiments. © *2008 American Institute of Physics.* [DOI: 10.1063/1.2976156]

I. INTRODUCTION

In the past decade, high throughput screening (HTS) has changed the way assays, such as binding, cellular processes, and motility, are performed.[1] Enthusiasm has separately yet simultaneously developed around manipulation and mechanical measurement of micro- and nanoscale systems, including cells[2] and single molecules.[3] This is because the mechanical properties of biological fluids and tissues are responsible for the structural integrity, function, and response of the organism.[4]

There has been little intersection between these two trends: low throughput techniques dominate mechanical study of biological systems. One high throughput nanomanipulation device, IBM's "Millipede" multitip atomic force microscope,[5] is a notable exception, but its primary application has been in data storage.

Among the systems for nanomanipulation, techniques using microbeads (particles $\sim 0.1-10$ μm) have been widely applied. Microbeads are used to measure mechanical properties of cells.[6–11] Drug delivery strategies are being developed using magnetic micro- and nanoparticles.[12] Transfection efficiency has been improved using "magnetofection," where vectors are attached to magnetic particles that are pushed against cells by magnetic fields.[13]

Microbead experiments of various biomaterials—including cells, actin, and fibrin—are frequently interpreted using the language of microrheology.[14,15] It has been noted that microrheological measurements show promise as a technique for high throughput screening.[16] We note that among microbead techniques, the "active" or "driven" techniques, where an external force is applied to a bead, can measure a wider range of moduli and are generally more flexible than the passive techniques, where the bead motion is due to thermal diffusion. Driven microrheology instrumentation includes laser traps ("optical tweezers") and paramagnetic attraction ("magnetic tweezers"). A laser trap offers high spatial resolution and can be precisely calibrated.[17] A magnetic system can drive multiple beads simultaneously, produce higher forces at a given bead size, and will neither heat nor otherwise interact with most biological specimens.[18]

In pursuit of HTS nanomanipulation, we have expanded on instrumentation to magnetically drive microbeads. Here we demonstrate a biocompatible, multiwell magnetic force system compatible with HTS standards. This magnetic high throughput system (MHTS) can apply forces of ~ 1 pN -1 nN. It is based on a standard microplate geometry and is designed to be scalable to 96 wells. We demonstrate that this technology can be used to measure mechanical properties of cells. MHTS technology is a key step toward a high throughput screening system for micro- and nanoscale biophysical experiments.

a)Electronic mail: rsuper@physics.unc.edu.

II. MHTS DESIGN AND FABRICATION

A. Magnetics miniaturization and temperature control

Applying force to magnetic beads requires a magnetic field gradient. For an initially unmagnetized, permeable magnetic bead, the force on the bead is

$$\mathbf{F} = \nabla(\mathbf{m} \cdot \mathbf{B}) = \frac{\pi d^3}{4\mu_0} \frac{\mu_r - 1}{\mu_r + 2} \nabla (B^2),$$

where $\mathbf{m}$ is the magnetic moment of the bead, d is its diameter, μ_r is its relative permeability, and B is the flux density of the ambient magnetic induction $\mathbf{B}$, as discussed in a previous work on a three-dimensional force microscope (3DFM).[19] This relation is valid until the bead becomes fully magnetized at a saturation magnetization M_{sat}, where

$$\mathbf{m} = \frac{\pi d^3}{6} M_{\text{sat}} \hat{\mathbf{m}},$$

where $\hat{\mathbf{m}}$ is the unit vector along $\mathbf{B}$. With the bead saturated, the force equation simplifies to

$$\mathbf{F} = \frac{\pi d^3}{6} M_{\text{sat}} \nabla B.$$

We desire a large magnetic field gradient to achieve high forces. In our work on the 3DFM and in Ref. 20, we employ a magnetic circuit design to achieve sufficient field gradient. Current-carrying drive coils magnetize a *drive core*, which preferentially directs magnetic flux to a *pole* of magnetic foil. The foil tapers to a pointed tip that sits submerged in the specimen. The magnetic flux travels through the specimen across a submillimeter gap back to a blunt segment of foil, the *flat*, where it returns to the common magnetic potential at the base of the drive core.

Collectively, the pole and flat are called a *pole flat*; this geometry can pull only toward the pole tip. Alternate pole geometries may be used for experiments that require different force fields. This thin-foil design accommodates a high numerical aperture, short working distance imaging objective, enabling high resolution imaging simultaneously with force application.

The present instrument, a MHTS, consists of two components: (1) a *magnetics block*, which generates magnetic flux for each well, and (2) a *magnetic microplate*, a custom-designed high throughput tray that incorporates a pole flat in each specimen well. The arrangement of these components is summarized in Fig. 1. The magnetics block contains a system of drive cores and drive coils; we report here on a 16-well prototype with a design that is scalable to 96 wells.

1. The magnetics block

Generating magnetic forces requires a complete magnetic system: drive coil, drive core, and magnetic return path. Figure 2 demonstrates how a complete magnetic system can fit within the area of one Society for Biomolecular Screening (SBS) microplate well. Each of the 16 magnetic systems includes a drive core and two *ears* that provide the magnetic return path. The magnetics block also has 16 through holes for brightfield illumination of the wells. To direct magnetic flux to the poles, the drive cores and ears extend past the bottom of the coils, so that when the magnetics block drops into the microplate, the drive cores and ears contact the pole flats at the bottom of the wells. The magnetics block is machined from a blank of ASTM A848 low-carbon magnetic iron. The drive coils are 58 turns of No. 26 AWG magnet wire, Part No. UNC-1 (Quality Coils, Inc., Bristol, CT).

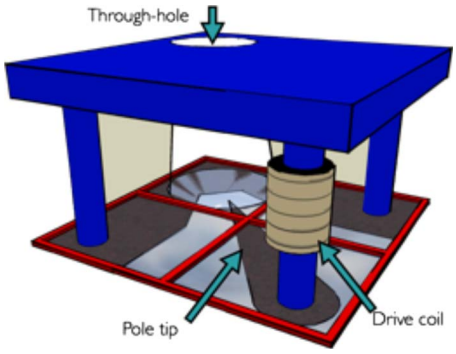

FIG. 1. (Color online) A cartoon of a single well's magnetic system. The substrate is a pole flat affixed to glass. The quadrants on the substrate show the footprint of a 2×2 section of the 384-well tray. The three-legged structure is the corresponding section of the magnetics block. A magnetic circuit begins in the drive coil (front well), where current creates magnetic flux directed by the drive core into the pole. Flux jumps the specimen gap (back well) to the flat, which is connected by two return path ears (left and right wells) to the back of the coil. By changing the etching pattern in the specimen gap (back well), the force field can be changed. A through hole above the specimen gap provides access for dosing of the specimen during an experiment and illumination for brightfield transmission microscopy.

Both biology and rheology are highly temperature sensitive, so we have built a temperature control system into the magnetics block. Fluid channels are drilled transversely to the optical paths, and aluminum manifolds are attached to the sides of the block as an interface to a heat exchanger and recirculation pump. In the limiting condition of all 16 wells at a maximum drive current, the temperature rise is 4 °C and the time constant is less than 1 min. The flow rate is within the laminar flow region of the channels, as calculated using a Moody chart.[21]

2. Fabrication of a biocompatible magnetic microplate

While we can place the magnetics above the specimen, the poles must be built into the HTS microplate. This constraint has three motivations. First, the force on beads increases with the pole tip's proximity to the specimen. Second, when using a pole flat, forces are applied in the plane of the pole tip, which to record bead motion must be parallel to the imaging plane. (For experiments requiring forces parallel to the imaging axis, alternate pole geometries may be implemented.) Third, a magnetic microplate can be washed and reused. It is relatively inexpensive, and so can be produced in quantity to allow for simultaneous preparation of many different experiments.

We assemble the magnetic microplate by adhering a pole plate underneath a bottomless plastic 384-well superstructure (Thermo Fisher Scientific, Portsmouth, NH). The pole plate is an array of 16 pole flats fixed to a 4.33×2.93 in.^{2} No. 1–thickness coverglass. We summarize the process in Fig. 3.

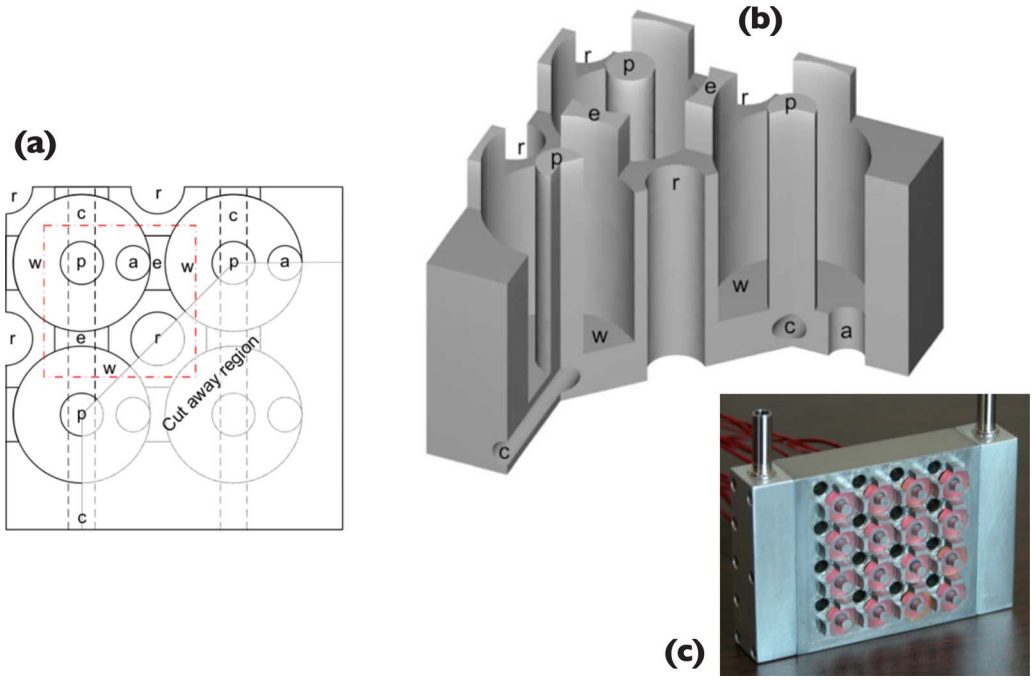

FIG. 2. (Color online) Schematics and a picture of the magnetics block; compare with the cartoon presented in Fig. 1. A magnetic system for a single well is outlined by a dashed square in schematic view (a). A cut-away perspective view is shown in (b). Within the area of one well in a 96-specimen microplate, the magnetics block houses two return path ears e, an optical relief r, a drive coil well w, and drive pole core p. Arranging the drive core on a diagonal from the specimen well and optical relief maximizes the volume for the drive coil. Heat transfer fluid channels c are drilled transversely to the optical paths, avoiding the coil wire access holes a. The 16-well prototype magnetics block is shown in (c), populated with drive coils and with aluminum manifolds mounted. The manifolds interface with a heat exchanger and recirculation pump.

We create the pole plate pattern using a commercial photolithographic etching process (Fotofabrication Corporation, Chicago, IL). The poles must be isolated from any surrounding magnetic material. Therefore, to maintain registration of these "floating" poles relative to the flats, we bond the 0.004 in. thick foil (Magnetic Shield Corporation, Bensenville, IL) to a sacrificial sheet of 0.005 in. thick polycarbonate backing (K-mac Plastics, Wyoming, MI). Here we report on an array of pole flats (see the inset of Fig. 3, step 2), but any shape of pole tip may be specified at this stage. The pole plate pattern is etched from the metal side of the foil on plastic.

To transfer the patterned foil to an optically clear substrate while maintaining the registration of the poles, we roll an UV-curable adhesive NOA 81 (Norland Optical Adhesives, Cranburg, NJ) onto the etched foil, cover it with No. 1–thickness coverglass, press flat with a glass plate and cure, then remove the plastic backing. This orientation places the sharp tip edge ~100 μm above the surface of the coverslip. A layer of parylene, vapor-deposited at this stage, inhibits pole degradation.

The highest force is in the plane of the pole edge, where the force ranges as high as ~1 nN on a 4.5 μm bead. This

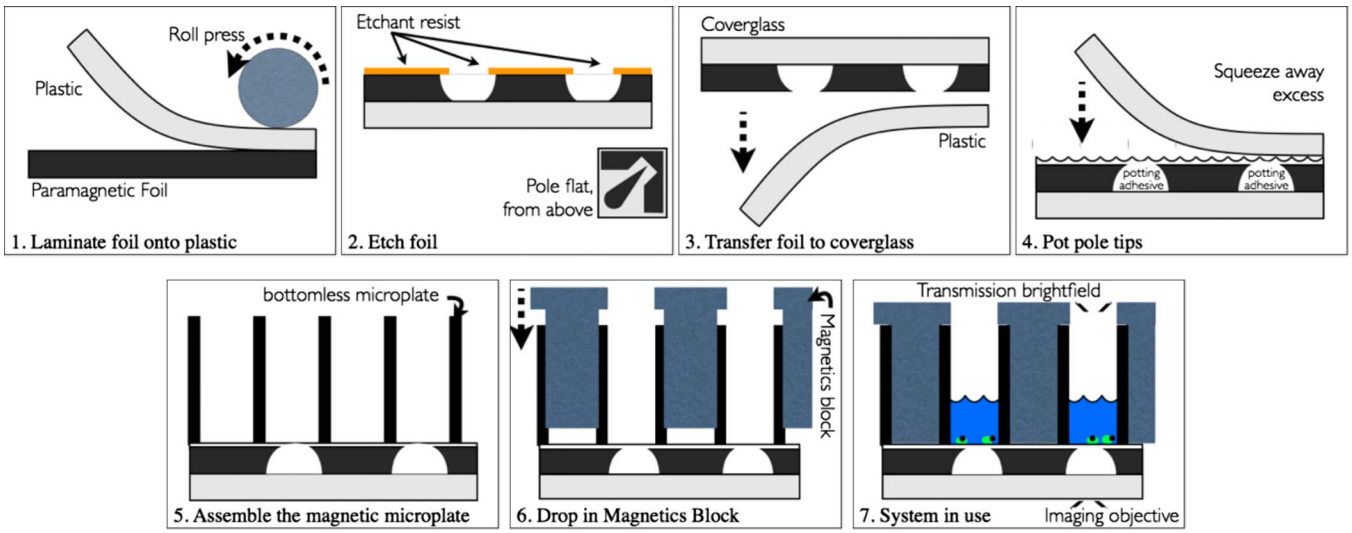

FIG. 3. (Color online) Magnetic microplate fabrication.

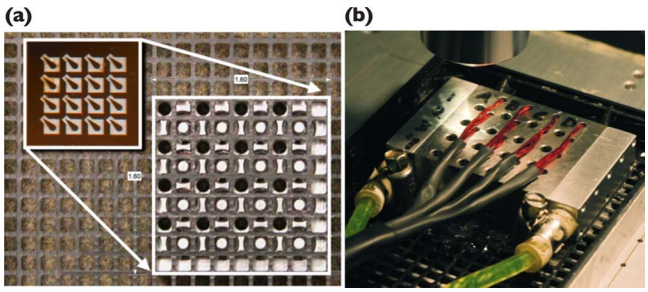

FIG. 4. (Color online) The fully assembled MHTS prototype. (a) Seen from below, the magnetics block drops into the 384-well microplate from above, and the pole plate creates the bottom of the specimen wells. (b) In operation, tubing provides fluid flow for temperature control, and a condenser objective provides transmission brightfield illumination from above. The imaging objective is below, obscured by the microplate.

geometry is desirable for some applications, including rheometry of biomaterials. For other applications, including cell force experiments, it is desirable to have the bottom of the well level with the pole. To raise the cells to this height, we pot the foil in NOA 81, creating an optically clear surface within 10 μm of the plane of the poles. To create a surface conducive to cell adhesion, we vapor deposit 3-aminopropyltriethoxysilane (Sigma-Aldrich, St. Louis, MO) solution onto the layer of NOA 81.

In the final step, Double/Bubble epoxy (V. O. Baker Co., Mentor, OH) epoxy bonds the potted pole plate to the 384-well superstructure such that the wells will not leak. The result is a 384-well microplate where three quarters of the wells are used for the drive cores and ears, leaving 96 wells for specimens. To elucidate the arrangement of the pole plate, well superstructure, and magnetics block, the fully assembled MHTS is shown in Fig. 4.

3. Considerations for MHTS operation

The MHTS technology described above comprises 16 independently controlled magnetic force generation systems. This instrument may be operated in a variety of modes. For example, identical forces may be applied simultaneously to a range of specimens by running the coils in series. Alternatively, different force profiles (say, pulses of varying length) may be applied to each well, limited by the number of current supplies available. In the present work, we use a computer-controlled transconductance current source;[20] manual switching runs this current in series through the desired coils.

The imaging subsystem in this work has a single field of view and a manual translation stage. Therefore, experiments that require a realtime record of bead motion must be performed sequentially. In addition, subsequent particle tracking and data analysis have been minimally automated. Nevertheless, experiments profit from the microplate geometry, which allows multiple specimens to be prepared simultaneously and more efficiently.

Using these nonautomated systems for a 15 s experiment, typical times are 2 min per well for data acquisition and 15 min per well for particle tracking and data analysis. Naturally, the MHTS technology presented here begs to be paired with existing HTS robotics and software. To this end, we are interested in implementing software to synchronize drive current commands with the position of a robotic microplate stage. The most urgent application for robotic data collection would be an automated force calibration routine. Additionally, control software to manage files associated with MHTS operation will greatly improve the utility of the MHTS. These files include force calibration, drive current, video logs, and subsequent tracking and analysis files.

III. FORCE CALIBRATION

The force field of an ideal pole can be modeled,[19] but deviation of manufactured tips from the model makes the prediction inadequate for precise force calibration. To address this problem, we have developed variable force calibration (VFC) software to construct the force field around the pole tip as a function of both distances from the pole tip r and the drive current I. We use VFC with the 3DFM to explore how forces are affected by the pole material, the drive current, and the bead position. We have also used VFC to calibrate the MHTS.

Forces are calculated from the velocity of beads pulled through a fluid of known viscosity. For Newtonian fluids with a low Reynolds number ($\mathrm{Re} < 10^{-4}$), the force on a spherical object is equal to the Stokes drag multiplied by the particle's velocity, $F = 6\pi a \eta v$, where a is the sphere radius, η is the dynamic viscosity of the fluid, and v is the sphere's velocity. Given the fluid viscosity and the bead radius, the bead's velocity uniquely determines the force at a given position and drive current.

Calibration is typically performed using 2.5M sucrose ($\eta = 0.12$ Pa s). Corn syrup (ACH Food Companies, Memphis, TN), a higher viscosity fluid ($\eta = 3.4$ Pa s), can be used to calibrate higher force regimes.

A. Variable force calibration in the 3DFM

1. Magnet control and voltage sequencing

A graphical environment, written in MATLAB, allows the user to drive the magnetic system with a series of constant-current pulses. A single *pulse sequence*, shown in Fig. 5, can be repeated as many times as necessary to collect sufficient calibration data.

The magnetic foil exhibits remanent magnetization after the application of a magnetic field. We can measure this hysteresis as a velocity of the magnetic bead at zero drive current. The remanence magnetization following the application of high drive current can mask subsequent low drive currents. To *degauss* the poles, we apply a drive current

$$I(t) = I_{\max} e^{-t/\tau} \sin 2\pi f t,$$

where $I_{\max}$ is the maximum applied current since the last degauss, τ is the decay time constant, and f is the frequency of the sinusoid. In the MHTS, $f = 1$ kHz and $\tau = 0.012$ s. Figure 6 shows the efficacy of this degauss technique.

2. Analysis pipeline

A datum of calibration is the bead's velocity at each drive current in each pulse sequence. Consider a population of n beads, which are each subjected to an average of p pulse

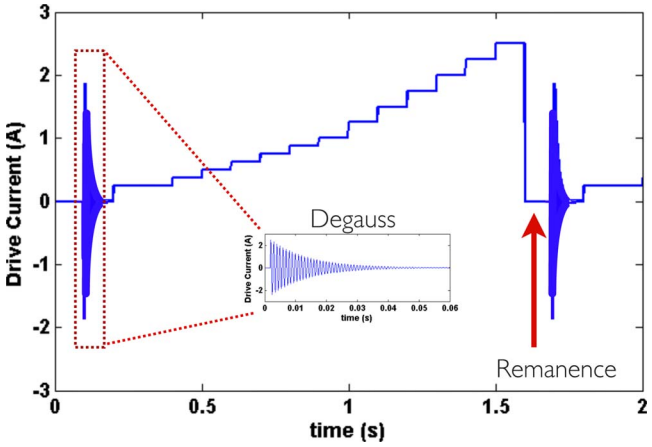

FIG. 5. (Color online) A pulse sequence beginning at zero drive current and rising to a final drive current of 2.5 A. Note the position of the degauss routine in the middle of the zero-current region. Comparing the pre- and postdegauss velocities of the bead demonstrates that the degauss routine eliminates force due to the remanent magnetization of the pole, as shown in Fig. 6. The inset shows a detail of the degauss routine.

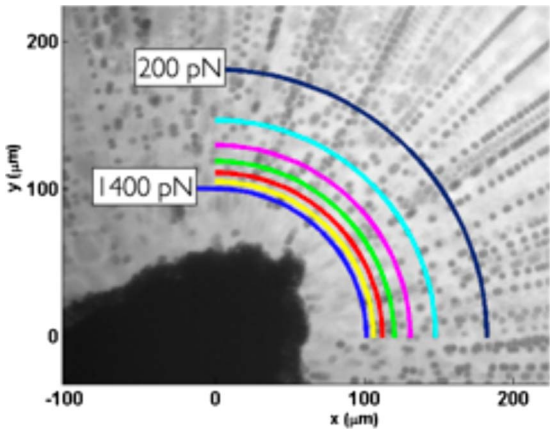

FIG. 7. (Color online) A contour plot of force on a 4.5 μm bead, overlaid on a time-lapse image of a force calibration video. The contour step is 200 pN. The pole tip (bottom left) is attracting beads from the surrounding solution, which are apparent as streaks in the time-lapse image. Each contour line is the average force measured on all beads at that distance from the pole tip, within 30° of the pole's axis of symmetry.

sequences. Each pulse sequence comprises d pulses at a specified drive current. A calibration set then includes npd data. Typical values are $n=20$, $p=10$, and $d=10$. We note that increasing d improves resolution in measuring how force varies with drive current; increasing n minimizes error due to bead-to-bead variation in force; shortening the dwell time of each pulse increases p and also moves the beads a shorter distance during each pulse sequence, thereby improving spatial resolution in the force calibration.

The only beads included in the analysis are those within an angle of $\pm 30°$ of the pole's line of symmetry, as the force varies significantly outside of that cone. The force field's radial symmetry is apparent in Fig. 7. We extend the bead trajectories to a point of common intersection within the area of the pole tip to determine the origin of this polar coordinate system. The coordinates of $[\boldsymbol{x}(t),\boldsymbol{y}(t)]$ are transformed into this system to find $\boldsymbol{r}(t)$. A linear fit to $\boldsymbol{r}(t)$ at each drive current I reveals the velocity $v(\boldsymbol{r},I)$.

The force data $\mathbf{F}$ may be displayed either as a function of $\boldsymbol{r}$ or as a function of the drive current at a given distance, $\mathbf{F}(I)$. The former representation is used in Fig. 6. The latter representation is used in Fig. 8 and provides insights into the pole plate material. At sufficient field strength, we expect the system's magnetic materials to achieve some maximum magnetization. This manifests as a saturation in the force on the beads as a function of current. Figure 8 shows the saturation behavior of two pole plate materials. The foil types are Netic ($B_{\mathrm{sat}}=2$ T) and CoNetic ($B_{\mathrm{sat}}=0.8$ T). As expected, the material with higher flux density saturation shows a higher force at saturation.

In Ref. 19 we argued that a pole tip can be modeled as a

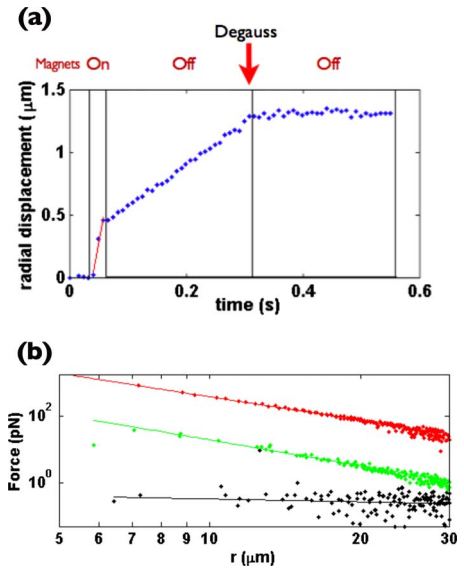

FIG. 6. (Color online) (a) Bead response to a characteristic pulse sequence. The drive current is on during the process in section I and is zero for sections II and III. Between sections II and III, the pole is degaussed. Note that at zero drive current, the bead's position continues to change. After degaussing, the bead position is constant. (b) The complete calibration set, plotted as $\mathbf{F}(\boldsymbol{r})$ for sections I (top curve), II (middle), and III (bottom). After degaussing, the force on the bead drops to within the noise created by bead diffusion.

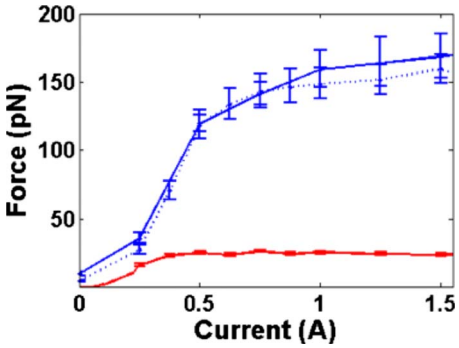

FIG. 8. (Color online) $\mathbf{F}(I)$ at a distance of ~ 10 μm from the edge of the pole tip for three calibration sets. This representation of the calibration demonstrates the saturation behavior of two μ-metals, Netic (top curve) and CoNetic (bottom curve). We also verify the validity of calibration by seeing the correspondence of Netic calibration using both 2.5M sucrose (dotted) and corn syrup (solid).

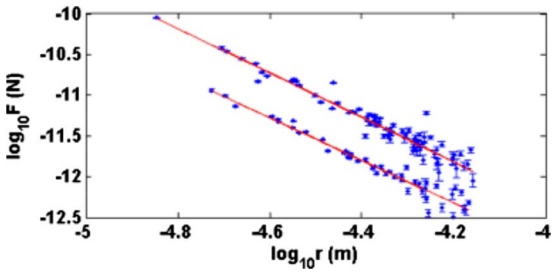

FIG. 9. (Color online) $\mathbf{F}(r)$ at drive currents $I=1.5$ A (top) and 0.25 A (bottom). Note that $\mathbf{F}\sim r^{-2.7}, r^{-2.6}$ for the top and bottom curves, respectively. The monopole model ($\mathbf{F}\sim r^{-3}$) overestimates the powerlaw because in reality the source of magnetic field is not confined to a single point, but it spreads over the volume of the pole tip.

magnetic monopole, such that $\boldsymbol{B}$ drops quadratically with distance from the monopole. Using the force equation for a saturated bead, we note that

$$\mathbf{F}\sim\nabla B\sim r^{-3}.$$

Figure 9 demonstrates powerlaw behavior of $\mathbf{F}\sim r^{-2.7}$. That the force model underpredicts the empirical powerlaw is encouraging. A real pole tip is not a magnetic monopole: it would more accurately be modeled as a distribution of magnetic charge. Such a distribution would have higher multipole moments than just the quadratic term, leading to a drop in the overall powerlaw.

B. MHTS calibration

We have used VFC to characterize the forces in the MHTS. Of greatest interest are the maximum force and crosstalk force. Figure 10 demonstrates that the maximum forces are ~1 nN, and with 15 wells on and one well off, the crosstalk is $3\pm1\%$.

Ideally, the pole tips would be uniform from well to well, ensuring identical force fields in all wells. However, the etching process that produces the pole plate pattern has not proven reliable in producing uniformly sized poles, and therefore the calibration varies from well to well by $\pm40\%$, as shown in Fig. 11. If this uncertainty is tolerable for the application, then a single calibration may be applied to data collected in all wells. If greater accuracy is desired, each well can be calibrated individually, resulting in a variation of $\pm10\%$. Calibration of a single well typically takes 3 min for data acquisition, 15 min for particle tracking, and 20 min for data analysis.

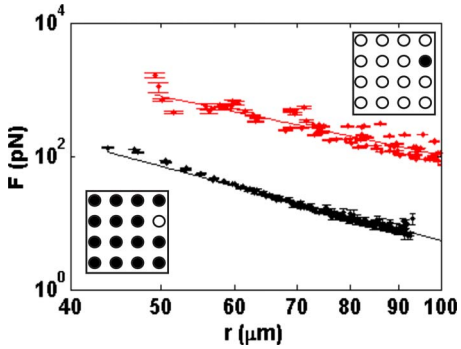

FIG. 10. (Color online) A representative calibration set for maximum force (top curve) and a calibration set showing crosstalk force (bottom curve) for a single well in the MHTS. The insets show the drive current configuration for each curve. For the maximum force calibration, the magnet in the active well is on and the other 15 are off; for the crosstalk measurement, the active well's magnet is off and the other 15 are on. The distance from the pole tip r is greater in the MHTS (Figs. 10 and 11) than that in the 3DFM (Figs. 6 and 9) because the MHTS pole tips are wider. This geometric difference results in a pole tip center that is farther from the edge of the pole tip.

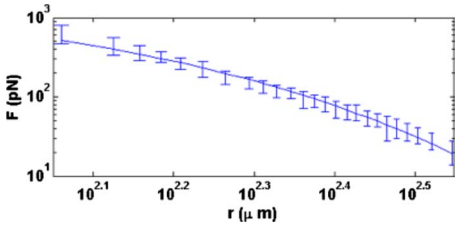

FIG. 11. (Color online) $\mathbf{F}(r)$ averaged over 15 wells in a MHTS magnetic microplate. One calibration set was collected at maximum drive current in each well ($d=1$). The forces in each well are uniform to within $\pm40\%$, which is adequate for some applications, including order-of-magnitude rheometry experiments.

IV. APPLICATION: MECHANICAL RESPONSE OF CELL MEMBRANE

There is a potential for a high throughput force system to have a dramatic impact on studies in cell mechanics and motility. For years, "cell rheology" has involved the study of biochemical and mechanical cellular responses under various mechanical (flow and prestress) and chemical (blockers and *p*H) conditions.[22,23] A recent trend in biological studies has been the development of libraries of small molecules, proteins, and RNAi for gene expression manipulation. These libraries offer enormous opportunities for understanding complex biochemical networks and for drug discovery, but impose daunting challenges to analytical techniques. A high throughput system can mitigate some of these challenges, including prep time, run time, and consistency in experimental procedure.

It has been a motivation for our development of the MHTS technology to explore gene-expression-inhibited and ligand-mediated cell mechanical responses of *Drosophila* (fruit fly) cell systems using a previously developed RNAi library.[22] Understanding these pathways will help reveal the genetic origins of diseases such as cancer, hypertension, and inflammatory disorders.

We have used the MHTS to study the mechanical response of cells under varying biochemistry. *Drosophila* derived cells (SR2+) were grown in SF 900 medium on potted, APTES treated, and Conconavalin A–washed magnetic microplates. That cell cultures grow in a magnetic microplate demonstrates MHTS biocompatibility; a representative well is shown in Fig. 12. The cultures were incubated at room temperature for 24 h before adding a suitable concentration of 2.8 μm volume-loaded superparamagnetic, COOH-functionalized beads (Invitrogen USA, Carlsbad, CA), which bind to the cell due to nonspecific electrostatic attraction. The cells were incubated for an additional hour, then washed to remove any unattached magnetic beads. Half of the wells with cells in them were treated with a protein tyrosine phos-

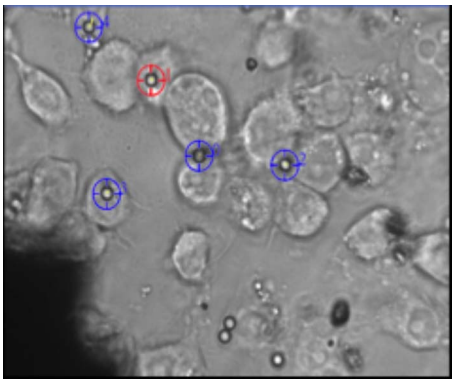

FIG. 12. (Color online) The magnetic microplate is compatible with cell cultures. The shadow of the pole tip is visible, bottom left. Shown is a brightfield transmission image of the *Drosophila* cells in the multiwell plate, 60×, 1.2 NA water immersion objective. Magnetic beads (d=2.8 μm) are observed on the cells and their trajectory is tracked using the CISMM VIDEO SPOT TRACKER software.

phatase (PTPase) inhibitor cocktail (Calbiochem, San Diego, CA), with a final concentration of 0.5 μM. Tyrosine phosphatases have been known to play an important role in force sensing in cells,[24] but there have been no quantitative studies on the changes in the mechanical properties of the cell due to the inhibition of PTPases.

Figure 13 compares the compliance of treated and untreated cells, as measured from bead displacements. A spring constant for a cell can be found by fitting the data to a modified Kelvin–Voigt model.[6] The spring constant for untreated *Drosophila* cells was $756 \pm 67 \times 10^{-6}$ N/m. SR2+ cells that were treated with the PTPase inhibitor showed greater compliance. The spring constant for cells treated with the PTPase inhibitor was found to be $240 \pm 53 \times 10^{-6}$ N/m.

Using the MHTS technology, a single experiment enabled mechanical measurements on cells in four independent cell cultures. The PTPase-treated SR2+ *Drosophila* cells exhibited thrice the compliance of control conditions; this difference is outside the uncertainty in the calibration of each well. Studies using the MHTS to study cell mechanoresponse under varying biochemical conditions are ongoing.

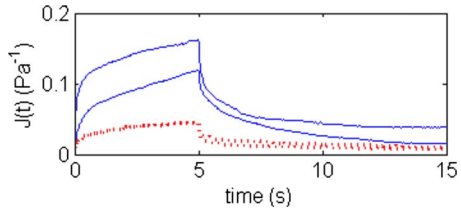

FIG. 13. (Color online) Compliance $J(t)=3\pi dr(t)/F(r,I)$ of individual *Drosophila* cells under control (dotted curves) and PTPase inhibited conditions (solid curves). Each curve represents a single bead on a single cell averaged over two pulls. All four beads were on cells in separate wells. The forces acting on the beads ranges from 20 to 350 pN.

V. CONCLUSIONS

We have presented critical technology for a MHTS based on commercial HTS standards and scalable to 96 wells. Our prototype applies independently controlled forces to 16 specimen wells. Force calibrations demonstrate forces in excess of 1 nN and reveal the saturation behavior of the magnetic pole material and expected force field dependence that approaches $\mathbf{F} \sim \boldsymbol{r}^{-3}$. We have demonstrated that MHTS technology can be used to perform cell manipulation experiments on independently prepared and treated cell cultures.

ACKNOWLEDGMENTS

The authors acknowledge parylene services provided by the Research Triangle Institute, Durham, NC. This work was supported by the National Institute of Biomedical Imaging and Bioengineering Grant Nos. P41-EB002025 and R01-EB000761.

[1] *Measuring Biological Responses with Automated Microscopy*, Methods in Enzymology Vol. 414, edited by J. Inglese (Elsevier, New York, 2006).
[2] P. Janmey and C. McCulloch, Annu. Rev. Biomed. Eng. **9**, 1 (2007).
[3] C. Bustamante, J. Macosko, and G. Wuite, Nat. Rev. Mol. Cell Biol. **1**, 130 (2000).
[4] Y.-C. Fung, *Biomechanics: Mechanical Properties of Living Tissues* (Springer, New York, 2005).
[5] U. Dürig, G. Cross, M. Despont, U. Drechsler, W. Häberle, M. Lutwyche, H. Rothuizen, R. Stutz, R. Widmer, P. Vettiger *et al.*, Tribol. Lett. **9**, 25 (2000).
[6] A. Bausch, W. Moller, and E. Sackmann, Biophys. J. **76**, 573 (1999).
[7] B. Fabry, G. Maksym, J. Butler, M. Glogauer, D. Navajas, and J. Fredberg, Phys. Rev. Lett. **87**, 148102 (2001).
[8] N. Wang, J. Butler, and D. Ingber, Science **260**, 1124 (1993).
[9] R. Hubmayr, S. Shore, J. Fredberg, E. Planus, R. Panettieri, W. Moller, J. Heyder, and N. Wang, Am. J. Physiol.: Cell Physiol. **271**, 1660 (1996).
[10] G. Lenormand, P. Bursac, J. Butler, and J. Fredberg, Phys. Rev. E **76**, 041901 (2007).
[11] T. Lele, J. Sero, B. Matthews, S. Kumar, S. Xia, M. Montoya-Zavala, T. Polte, D. Overby, N. Wang, and D. Ingber, Methods Cell Biol. **83**, 443 (2007).
[12] J. Dobson, Nanomedicine **1**, 31 (2006).
[13] C. Plank, U. Schillinger, F. Scherer, C. Bergemann, J. Rémy, F. Krötz, M. Anton, J. Lausier, and J. Rosenecker, Biol. Chem. **384**, 737 (2003).
[14] T. A. Waigh, Rep. Prog. Phys. **68**, 685 (2005).
[15] F. MacKintosh and C. Schmidt, Curr. Opin. Colloid Interface Sci. **4**, 300 (1999).
[16] V. Breedveld and D. J. Pine, J. Mater. Sci. **38**, 4461 (2003).
[17] K. Neuman and S. Block, Rev. Sci. Instrum. **75**, 2787 (2004).
[18] J. Fisher, L. Vicci, J. Cribb, E. O'Brien, R. Taylor, and R. Superfine, NANO **1**, 191 (2006).
[19] J. Fisher, J. Cribb, K. Desai, L. Vicci, B. Wilde, K. Keller, R. Taylor, J. Haase, K. Bloom, E. OBrien *et al.*, Rev. Sci. Instrum. **77**, 023702 (2006).
[20] J. Fisher, J. Cummings, K. Desai, L. Vicci, B. Wilde, K. Keller, C. Weigle, G. Bishop, R. Taylor, C. Davis *et al.*, Rev. Sci. Instrum. **76**, 053711 (2005).
[21] *Eschbach's Handbook of Engineering Fundamentals*, 4th ed., edited by B. D. Tapley (Wiley, New York, 1990).
[22] S. Rogers and G. Rogers, Nat. Protocols **3**, 606 (2008).
[23] M. Puig-de Morales, E. Millet, B. Fabry, D. Navajas, N. Wang, J. Butler, and J. Fredberg, Am. J. Physiol.: Cell Physiol. **287**, 643 (2004).
[24] G. Giannone and M. Sheetz, Trends Cell Biol. **16**, 213 (2006).